Supercond. Sci. Technol. **22** (2009) 015004 (5pp) doi:10.1088/0953-2048/22/1/015004

Josephson phase qubit circuit for the evaluation of advanced tunnel barrier materials

Jeffrey S Kline[1], Haohua Wang[2], Seongshik Oh[1,3], John M Martinis[2] and David P Pappas[1]

[1] National Institute of Standards and Technology, Boulder, CO 80305, USA
[2] Department of Physics, University of California, Santa Barbara, CA 93106, USA

E-mail: klinej@nist.gov

Received 23 September 2008, in final form 24 October 2008
Published 21 November 2008
Online at stacks.iop.org/SUST/22/015004

Abstract
We have found that crystalline Josephson junctions have problems with the control of critical current density that decrease the circuit yield. We present a superconducting quantum bit circuit designed to accommodate a factor of five variation in critical current density from one fabrication run to the next. The new design enables the evaluation of advanced tunnel barrier materials for superconducting quantum bits. Using this circuit design, we compare the performance of Josephson phase qubits fabricated with MgO and Al_2O_3 advanced crystalline tunnel barriers to AlO_x amorphous tunnel barrier qubits.

(Some figures in this article are in colour only in the electronic version)

1. Introduction

One of the greatest challenges in the development of a practical solid-state quantum computer is to overcome quantum decoherence due to unwanted coupling between the environment and the quantum bit (qubit) [1]. The performance of superconducting Josephson phase qubits is presently limited by decoherence due to microwave dielectric loss in both the tunnel barrier [2] and the wiring cross-over insulator [3]. Thus, the dominant sources of decoherence originate within the material components of the qubit itself. The dielectric loss in the tunnel barrier can be reduced by the use of advanced tunnel barrier materials [4] or by reducing the area of the high-loss tunnel junction [5]. Likewise, the dielectric loss in the wiring cross-over insulators can be reduced by the use of low-loss insulators [3, 6] or by reducing the volume of the high-loss insulator.

Optimization of the materials used in the tunnel barrier can improve qubit performance. For example, measurement fidelity of the ground and excited states ($|0\rangle$ and $|1\rangle$) of the qubit and the energy relaxation time T_1 improves as the number of spurious two-level states (TLSs) in the tunnel barrier decreases. TLSs are defect states with a non-zero electric dipole that dissipate energy in a resonant microwave electric field [7]. Oh *et al* demonstrated that the usage of a crystalline Al_2O_3 tunnel barrier reduces the density of TLSs by ∼80% compared to the ubiquitous amorphous AlO_x tunnel barrier [4]. This reduction in density of TLSs can be explained by the higher coordination number and crystallinity of Al_2O_3 compared to that of AlO_x.

The investigation of advanced tunnel barrier materials for qubits can be hindered by variations in the critical current density (J_c) from one deposition run to the next. We find that low leakage Re/Al_2O_3/Al and Re/MgO/Al Josephson junctions with crystalline tunnel barriers, where the barrier is fabricated by reactive evaporation [8], have a greater variation in J_c than do amorphous tunnel barriers fabricated by thermal oxidation of Al. This variation in J_c could be caused by variations in the tunnel barrier thickness due to instability in the reactive evaporation rate, or by the relatively smaller number of 'hot spots' [9] that are predicted for crystalline tunnel barriers [10]. Also, in the commonly used thermal oxidation technique for the fabrication of amorphous junctions, the thickness of the tunnel barrier depends logarithmically on the deposition time and is relatively insensitive to small variations in the oxidation time. In contrast, the reactive evaporation method is linear in

[3] Present address: Department of Physics and Astronomy, Rutgers, The State University of New Jersey, Piscataway, NJ 08854, USA.

time and is more sensitive to variations in the deposition time and evaporation rate.

The junction critical current (I_c) is related to J_c via $I_c = J_c A$, where A is the junction area, and may vary from 1 to 5 μA for 5 μm $\times$ 5 μm junctions, from one deposition run to the next, where the tunnel barrier deposition conditions are the same for each run. This variation in I_c by a factor of five makes it difficult to fabricate a working qubit circuit that requires I_c in the range 1.1–2.8 μA.

To circumvent the issues in control of the critical current density associated with crystalline tunnel junctions and presumably other advanced tunnel junctions, we have designed a qubit circuit that can accommodate the above-mentioned variation in junction critical current. This circuit design is useful for evaluating advanced tunnel barrier materials where the control of critical current density may not be as good as that for established tunnel barrier technologies.

2. Fabrication and processing

We fabricated the qubit circuits on crystalline Al_2O_3(0001) substrates (12.7 mm $\times$ 15 mm $\times$ 0.43 mm) using an epitaxial trilayer process described in [8]. Briefly, the trilayer consists of a crystalline rhenium base electrode 160 nm thick, a crystalline Al_2O_3 or MgO tunnel barrier $\sim$1.5 nm thick, and a polycrystalline aluminum top electrode 100 nm thick. The base electrode is deposited at high substrate temperature ($\sim$1100 K) by sputtering. The tunnel barrier is grown by reactive evaporation of Al or Mg in a molecular oxygen background (10^{-4} Pa) at room temperature. In addition, the Al_2O_3 tunnel barrier requires a post-growth high-temperature anneal ($\sim$1050 K) for crystallization. The top electrode is deposited by evaporation at room temperature.

We performed lateral trilayer patterning using optical lithography, ion milling and plasma- and wet-etching techniques. The wiring cross-over insulator is amorphous SiO_2, 360 nm thick, deposited by plasma enhanced chemical vapor deposition at room temperature. The volume of the high-loss SiO_2 insulator [11] has been minimized by retaining it only where necessary for the separation of wiring layers. This is accomplished by the use of a self-aligned reactive ion etch of SiO_2 after the completion of the Al wiring (100 nm thick, sputter deposited at room temperature) layer patterning.

3. Circuit design

The individual qubit circuit is similar to the design described in [12]. It consists of a flux biased Josephson phase qubit with a Josephson junction in a gradiometer loop. An overlapped gradiometer three-junction direct current superconducting quantum interference device (SQUID) with 64 pH mutual inductance between the qubit and SQUID loop is used for qubit state readout measurement, as shown in figure 1. The three-junction SQUID design is used so that the SQUID–qubit coupling can be modulated. One branch of the SQUID loop has a single Josephson junction with critical current $I_c = 1.6$ μA and capacitance $C \sim 2$ pF, and the other branch has two larger junctions, each with critical current 1.7 $\times$ I_c. The qubit loop

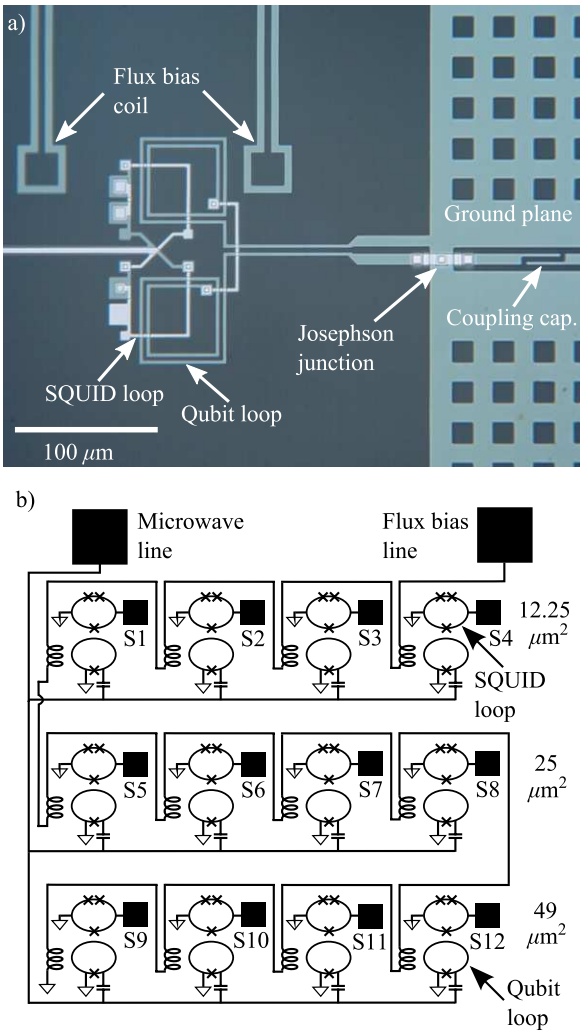

Figure 1. Optical and schematic views of the qubit circuit. (a) Micrograph of an individual qubit circuit consisting of a Josephson junction in a gradiometer loop, state readout measurement SQUID and gradiometric flux bias coil. The perforated ground plane and microwave coupling capacitor are visible at the right. (b) Schematic drawing of the full 12-qubit circuit with qubit junction areas listed at the right. The microwave lines and flux bias lines are common to all 12 qubit circuits, while the SQUID bias lines S1–S12 are individually biased for each circuit.

with inductance $L = 722$ pH is sensitive to the flux bias coil through mutual inductance $M = 2.67$ pH, but the SQUID loop has negligible mutual inductance, due to its symmetric position with respect to the gradiometric flux bias coil.

The qubit and SQUID Josephson junctions are square. The smallest linewidth and line spacing of the wires are 2 μm and 1.5 μm, respectively. A perforated ground plane with 10 μm $\times$ 10 μm holes is used to immobilize the trapped magnetic flux. The flux bias coil and qubit loop are fabricated primarily from base layer material (Re) and the SQUID loop is fabricated primarily from wiring layer material (Al). The usage of Re, which does not readily oxidize, for the qubit loop may reduce the $1/f$ flux noise in the qubit [13] due to the reduced number of TLSs in the native oxide of the superconductor [14].

The unintentional variation in critical current density of our crystalline Josephson junctions makes proper circuit

Table 1. Qubit performance comparison between three different Josephson phase qubits. The loss tangent $\tan\delta$ of the tunnel barrier and cross-over insulator (measured at single photon energy), defect density σ and qubit area A all affect the measured energy relaxation time T_1.

Tunnel barrier			Cross-over insulator		Qubit	
Material	$\tan\delta$	σh (μm^2 GHz)$^{-1}$	Material	$\tan\delta$	A (μm^2)	T_1 (ns)
a-AlO_x	10^{-3} [3]	0.5	SiN_x	10^{-4} [11]	13	500 [3]
c-MgO	10^{-3} [11]	0.4	SiO_2	10^{-3} [11]	25	80
c-Al_2O_3	10^{-5} [11]	0.2	SiO_2	10^{-3} [11]	49	500

operation a challenge. Many deposition systems equipped with *in situ* surface characterization equipment suitable for advanced tunnel barrier growth and characterization can only accommodate small chip-sized (∼1 cm × 1 cm) substrates, as opposed to traditional deposition systems that may utilize wafers 75 mm in diameter or larger. To obtain the highest possible yield of qubit devices on a small 12.5 mm × 15 mm chip that contains only two dies, we placed 12 qubit circuits on each 6 mm × 6 mm die. This amounts to an increase of three times as many qubit circuits compared to a previous crystalline qubit study [4].

To accommodate the variation in I_c by 1 to 5 μA from one deposition to the next, we utilize circuits designed to operate with different target critical current densities. This is accomplished by varying the qubit junction area (12.25, 25 and 49 μm^2) so that we have four qubit circuits of each size on a single die. We deliberately use junctions of large area so that we can obtain meaningful statistics on the TLS density of advanced tunnel barrier materials. The respective circuits are designed with a target $I_c = 1.6$ μA. The area of the small SQUID junction matches the qubit junction area, and the larger SQUID junctions are scaled by a factor of 1.7. Assuming that J_c is uniform over the entire die, only four circuits of one particular size will have the proper I_c on a given die (e.g., four 25 μm^2 size circuits are operable, but 12.25 and 49 μm^2 sized circuits have I_c outside the desired range).

To accommodate the large number of qubit circuits per die, we utilize capacitively coupled microwave lines ($C = 0.5$ fF) and inductively coupled flux bias lines common to all 12 qubit circuits. The flux bias lines are connected in series to each separate qubit circuit, as shown in figure 1(b). During normal operation, all 12 qubits are subjected to flux bias and microwave radiation on the common lines, but the SQUID bias lines are individually controlled for state readout of only one qubit at a time.

The actual qubit junctions are inaccessible for direct measurements of critical current because they are shunted by the qubit inductive loop. For measurement of the critical current, we placed eight isolated test junctions with wiring suitable for four-probe measurements around the perimeter of the die. After fabrication, we perform room-temperature four-probe measurements of the normal state resistance R_n of the junctions as an initial screening test for critical current using the Ambegaokar–Baratoff formula [15]

$$I_c = \frac{\pi}{2eR_n}\Delta(T)\tanh\left(\frac{\Delta(T)}{k_BT}\right),$$

where e is the electron charge, T is the temperature, Δ is the superconducting energy gap and k_B is Boltzmann's constant.

4. Low-temperature measurements

We first perform low-temperature ($T = 75$ mK) measurements of the SQUIDs in an adiabatic demagnetization refrigerator (ADR), which requires considerably fewer operational resources than does a dilution refrigerator. We measure SQUID IV curves and SQUID–qubit switching curves in the ADR to check for proper operation of the SQUID and the critical current of the qubit junction. Next we cool the die in a dilution refrigerator ($T = 20$ mK) where microwave lines are available.

We plot the peak value of the occupation probability of the qubit $|1\rangle$ state in figure 2(a) as a function of excitation frequency and qubit bias. Along with the expected bias dependence, we find anomalous avoided two-level crossings (splittings) in the spectroscopy that result from the qubit resonating with individual TLSs in the tunnel barrier [2]. A comparison of the splitting distribution between qubits with amorphous AlO_x (a-AlO_x, data averaged over seven samples), crystalline Al_2O_3 (c-Al_2O_3, data averaged over three samples) and crystalline MgO (c-MgO, data averaged over two samples) tunnel barriers is shown in figure 2(b). The initial sloped portion of the curves can be approximated by the relation[4]

$$\frac{dN}{dE}(S') - \frac{dN}{dE}(0.01) \approx 2.30\sigma A\left[\log S' + 2\right],$$

where $\frac{dN}{dE}$ is the integrated density of splittings with size S/h between 0.01 GHz and S'/h, h is Planck's constant and σ is a material constant describing the TLS defect density [3]. We assume that any splittings smaller than the arbitrarily assigned 0.01 GHz cutoff frequency are artifacts. However, the choice of cutoff frequency does not affect the slope of the curves, 2.30 σA.

As summarized in table 1, we find that σ of the crystalline Al_2O_3 tunnel barrier is one third as large as that of the amorphous AlO_x barrier. This corresponds to a 60% reduction in the TLS density and agrees reasonably well with the 80% reduction of [4] obtained from counting the number of TLSs in the spectroscopy data. Comparisons between σ are more accurate than comparisons between the number of splittings, which depend on the choice of cutoff frequency.

The crystalline MgO qubit had only a slight reduction in σ compared to that of the amorphous AlO_x qubit. We attribute

[4] This equation was derived by neglecting the square-root term in equation (4) of [3], integrating with respect to S and evaluating from the limits 0.01 GHz to S'.

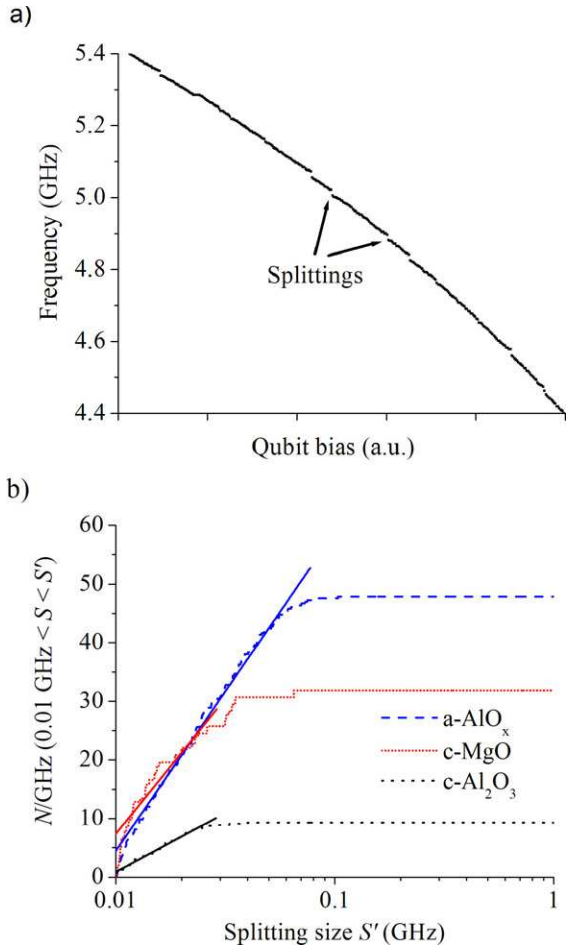

Figure 2. Measurement of the qubit–TLS interaction. (a) Spectroscopy of the $|0\rangle \rightarrow |1\rangle$ qubit transition as a function of qubit bias for the c-Al_2O_3 qubit. (b) Size distribution of the TLSs in 49 μm^2 junctions normalized to a 1 GHz bandwidth. Based on the slope of the fitted solid lines, σh, the material constant describing the TLS defect density is 0.2, 0.4 and 0.5 (μm^2 GHz)$^{-1}$ for the c-Al_2O_3, c-MgO and a-AlO_x tunnel barriers, respectively.

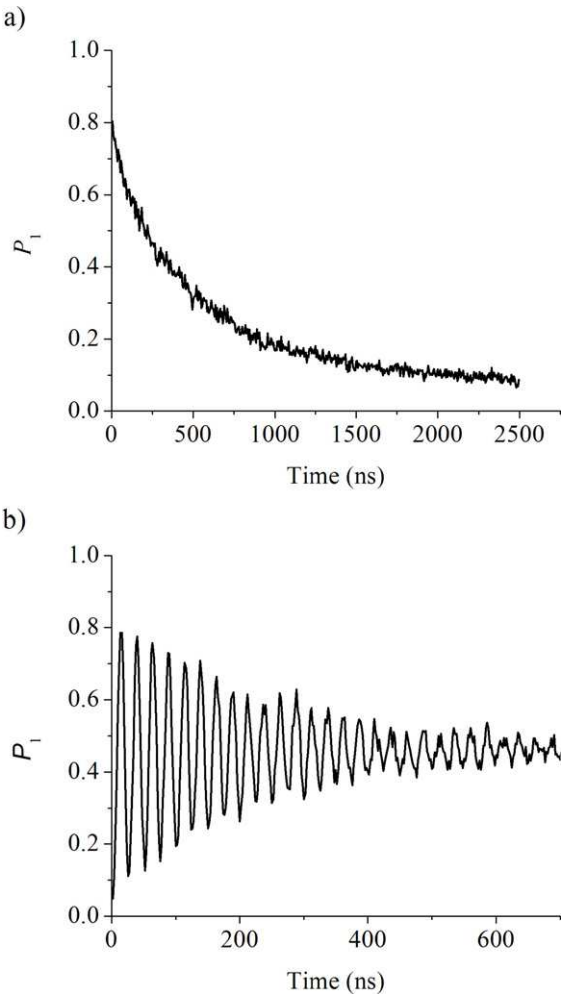

Figure 3. Low-temperature ($T = 20$ mK) measurements for the qubit with a c-Al_2O_3 tunnel barrier. (a) Energy relaxation time $T_1 = 500$ ns. Measurement fidelity = 80%. (b) Rabi oscillations: dephasing time $T_2 \sim 140$ ns. Rabi visibility = 70%.

this to the large lattice mismatch (8%) between the Re base electrode and MgO tunnel barrier, resulting in a large density of defect sites and hence TLSs.

Measurement of the energy relaxation time of the $|1\rangle$ state to the ground state for the 49 μm^2 crystalline Al_2O_3 qubit yielded 500 ns. The measurement fidelity is ~80% and the dephasing time $T_2 \sim 140$ ns, extracted from the Rabi oscillations shown in figure 3. These values are comparable to the results obtained from the smaller 13 μm^2 amorphous AlO_x qubit fabricated with SiN_x insulator [3], which has a 10× lower loss tangent than SiO_2. This indicates that a small-area (13 μm^2) crystalline Al_2O_3 qubit would have improved energy relaxation time and measurement fidelity due to the decreased number of TLSs that are expected.

The energy relaxation time of the crystalline MgO qubit is significantly shorter than that for a-AlO_x and c-Al_2O_3, as shown in table 1. The TLS density σ is similar for MgO and AlO_x, so the MgO qubit should have had a comparable T_1 if dielectric loss were the only loss mechanism present. The short T_1 of the MgO qubit may be due to phonon radiation in the tunnel barrier [16]. This is supported by the fact that MgO has piezoelectric constants similar to those of AlN, which was shown to have a short ~20 ns energy relaxation time when used as a tunnel barrier material [17].

5. Conclusions

We have presented a Josephson junction phase qubit circuit design that accommodates a variation in critical current density by a factor of five from one deposition run to the next. This design proved to be useful in the early investigation of advanced tunnel barrier materials for quantum computation applications where process control of the junction critical current density has not yet been optimized. Using the new circuit design, we compared the performance of Josephson phase qubits fabricated with MgO and Al_2O_3 advanced crystalline tunnel barriers to that of AlO_x amorphous tunnel barrier qubits.

Acknowledgments

This work was funded by the US government and IARPA.

References

[1] Nielsen M A and Chuang I L 2000 *Quantum Computation and Quantum Information* (Cambridge: Cambridge University Press)

[2] Simmonds R W, Lang K M, Hite D A, Nam S, Pappas D P and Martinis J M 2004 Decoherence in Josephson phase qubits from junction resonators *Phys. Rev. Lett.* **93** 077003

[3] Martinis J M *et al* 2005 Decoherence in Josephson qubits from dielectric loss *Phys. Rev. Lett.* **95** 210503

[4] Oh S, Cicak K, Kline J S, Sillanpää M A, Osborn K D, Whittaker J D, Simmonds R W and Pappas D P 2006 Elimination of two level fluctuators in superconducting quantum bits by an epitaxial tunnel barrier *Phys. Rev.* B **74** 100502(R)

[5] Steffen M, Ansmann M, McDermott R, Katz N, Bialczak R C, Lucero E, Neeley M, Weig E M, Cleland A N and Martinis J M 2006 State tomography of capacitively shunted phase qubits with high fidelity *Phys. Rev. Lett.* **97** 050502

[6] Neeley M, Ansmann M, Bialczak R C, Hofheinz M, Katz N, Lucero E, O'Connell A, Wang H, Cleland A N and Martinis J M 2008 Process tomography of quantum memory in a Josephson-phase qubit coupled to a two-level state *Nat. Phys.* **4** 523–6

[7] Hunklinger S and Schickfus M 1981 Acoustic and Dielectric properties of Glasses at low temperatures *Amorphous Solids: Low-Temperature Properties* (*Topics in Current Physics* vol 24, ed K V Lotsch) ed W A Phillips (Berlin: Springer) pp 81–106

[8] Oh S, Cicak K, McDermott R, Cooper K B, Osborn K D, Simmonds R W, Steffen M, Martinis J M and Pappas D P 2005 Low-leakage superconducting tunnel junctions with a single-crystal Al_2O_3 barrier *Supercond. Sci. Technol.* **18** 1396–9

[9] Dorneles L S, Schaefer D M, Carara M and Schelp L F 2003 The use of Simmons' equation to quantify the insulating barrier parameters in $Al/AlO_x/Al$ tunnel junctions *Appl. Phys. Lett.* **82** 2832–4

[10] Raikh M E and Ruzin I M 1991 Transmittancy fluctuations in randomly non-uniform barriers and incoherent mesoscopics *Mesoscopic Phenomena in Solids* (*Modern Problems in Condensed Matter Sciences* vol 30, ed V M Agranovich and A A Maradudin) ed B L Altshuler *et al* (Amsterdam: Elsevier) pp 315–68

[11] O'Connell A D *et al* 2008 Microwave dielectric loss at single photon energies and millikelvin temperatures *Appl. Phys. Lett.* **92** 112903

[12] Neeley M, Ansmann M, Bialczak R C, Hofheinz M, Katz N, Lucero E, O'Connell A, Wang H, Cleland A N and Martinis J M 2008 Transformed dissipation in superconducting quantum circuits *Phys. Rev.* B **77** 180508(R)

[13] Sendelbach S, Hover D, Kittel A, Mück M, Martinis J M and McDermott R 2008 Magnetism in SQUIDs at millikelvin temperatures *Phys. Rev. Lett.* **100** 227006

[14] Gao J, Daal M, Vayonakis A, Kumar S, Zmuidzinas J, Sadoulet B, Mazin B A, Day P K and Leduc H G 2008 Experimental evidence for a surface distribution of two-level systems in superconducting lithographed microwave resonators *Appl. Phys. Lett.* **92** 152505

[15] Ambegaokar V and Baratoff A 1963 Tunneling between superconductors *Phys. Rev. Lett.* **10** 486–9

[16] Ioffe L B, Geshkenbein V B, Helm C and Blatter G 2004 Decoherence in superconducting quantum bits by phonon radiation *Phys. Rev. Lett.* **93** 057001

[17] Bialczak R, Ansmann M, Katz N, Lucero E, McDermott R, Neeley M, Steffen M, Weig E, Cleland A and Martinis J 2006 Fabrication and testing of AlN Josephson junction qubits *American Physical Society March Mtg (Baltimore, MD)*